Level Set Segmentation of Optic Discs from Retinal Images

Chuang Wang, Djibril Kaba, and Yongmin Li
Department of Computer Science, Brunel University, London, UK
Email: {Chuang.Wang, Djibril.Kaba, Yongmin.Li}@brunel.ac.uk

Abstract—**Analysis of retinal images can provide important information for detecting and tracing retinal and vascular diseases. The purpose of this work is to design a method that can automatically segment the optic disc in the digital fundus images. The template matching method is used to approximately locate the optic disc centre, and the blood vessel is extracted to reset the centre. This is followed by applying the Level Set Method, which incorporates edge term, distance-regularization term and shape-prior term, to segment the shape of the optic disc. Seven measures are used to evaluate the performance of the methods. The effectiveness of the proposed method is evaluated against alternative methods on three public data sets DRIVE, DIARETDB1 and DIARETDB0. The results show that our method outperforms the state-of-the-art methods on these datasets.**

Index Terms—**active contours, optic disc segmentation, retinal image, level sets, template matching**

I. INTRODUCTION

Glaucoma, predicted to affect about 70 million people around the world by 2020 [1], is one of the major causes of blindness in the world. This disease manifests by gradual degeneration of the retinal ganglion cell axons and cupping of the disc, thus the optic disc nerve is an important structure in glaucoma analysis. Over the past years, glaucoma experts have analysed the amount of cupping using manual planimetry on stereo colour photographs of the optic disc nerve, where the boundary of the optic disc is labelled. However, the manual planimetry of the optic disc nerve is time consuming and can be exposed to human error. Thus, a reliable automated method for the optic disc segmentation, which preserves various optic disc shapes, is attractive in computer aided-diagnosis and suitable for large-scale retinal disease screening.

In the literature, numerous studies have been published on automated segmentation of the optic disc. The shape based template matching is one of the earliest methods used for the optic disc segmentation. This method models the optic disc as a circular or elliptical object [2]-[7]. The performance of this technique is affected by the presence of the blood vessels inside the optic disc region. To overcome these limitations, the blood vessels are removed by using morphological operation in [2].

Nevertheless, the shape based modelling approach of the optic disc extraction is not effective due to the intensity inhomogeneity and the change of the disc shape by the exudates present in abnormal images.

To address the problem of shape irregularity and intensity inhomogeneity, several gradient based active contour methods have been developed [8]-[10]. Those methods initialise the contour automatically or manually and performed the deformation of the contour with an energy functional derived by the image gradient. Then a gradient vector flow based contour model is used to detect the optic disc boundary, and the energy functional is minimised with respect to the high gradient of the vessels. This process is achieved using pre-processing step of incorporating a circular or elliptical shapes into the segmentation algorithm. To further improve the active contour method by handling the local gradient minima, a variational level set based deformable model was developed to smooth the segmentation with an ellipse fitting operation [11]. This process either incorporates the shape model into the energy formulation or uses a post-processing step. However, a limitation of this method is that it constraints the extraction range of irregular optic disc region.

A model free snake methods [12]-[14] are developed to effectively segment any irregular disc shape using a supervised classification. These methods classify all the contour points as edge point cluster or uncertain point cluster after each deformation [15]. The uncertain point cluster groups all the pixel points belonging to the blood vessels and the segmentation is only performed on edge point cluster considered as disc pixels. To address the local gradient variation, the deformation of each point used global and local information. Though this method produces good segmentation results on normal and irregular optic disc shape, the segmentation accuracy is far more sensitive to the contour initialisation.

The model proposed by Shah et al. [16] has been widely used in region based active contour to overcome the local gradient variation, the sensitivity to contour initialisation and the noise. This region based active contour approach [17] applies statistical models to define both the foreground and the background before minimising the energy functional. For example, the method proposed in [18] achieved a good segmentation performance but it was unable to accurately segment the boundary of images with smooth region transition between the optic disc area and the background. To

address this problem, the Chan-Vese method [17] was incorporated with a circular shape into the segmentation formulation. Tang *et al*. [19] developed an automatic method to segment the papilla using the combination the Chan-Vese model and an elliptic shape restraint to ensure that the evolving curve stays an ellipse. Though this method shows a good performance in detecting the papilla shapes, restricting the segmentation to an elliptic shape may adversely affect the segmentation of irregular optic disc shapes.

In order to improve the segmentation of the optic disc boundary, we present in this paper a novel method by combining the template matching model and the Level Set Method. The segmentation formulation incorporates

edge, distance-regularization and shape-prior terms respectively, making it possible to segment the optic disc with large gradient distraction near the boundary and preserve various optic disc shapes.

II. OPTIC DISC CENTRE DETECTION

Inspired by the method reported by the Lowell et al. [8], the template matching method is used to locate the approximate optic disc centre. Fig. 1 shows the process to locate the optic disc centre. There are two main stages for the optic disc centre detection: (1) template matching, and (2) relocating the optic disc centre.
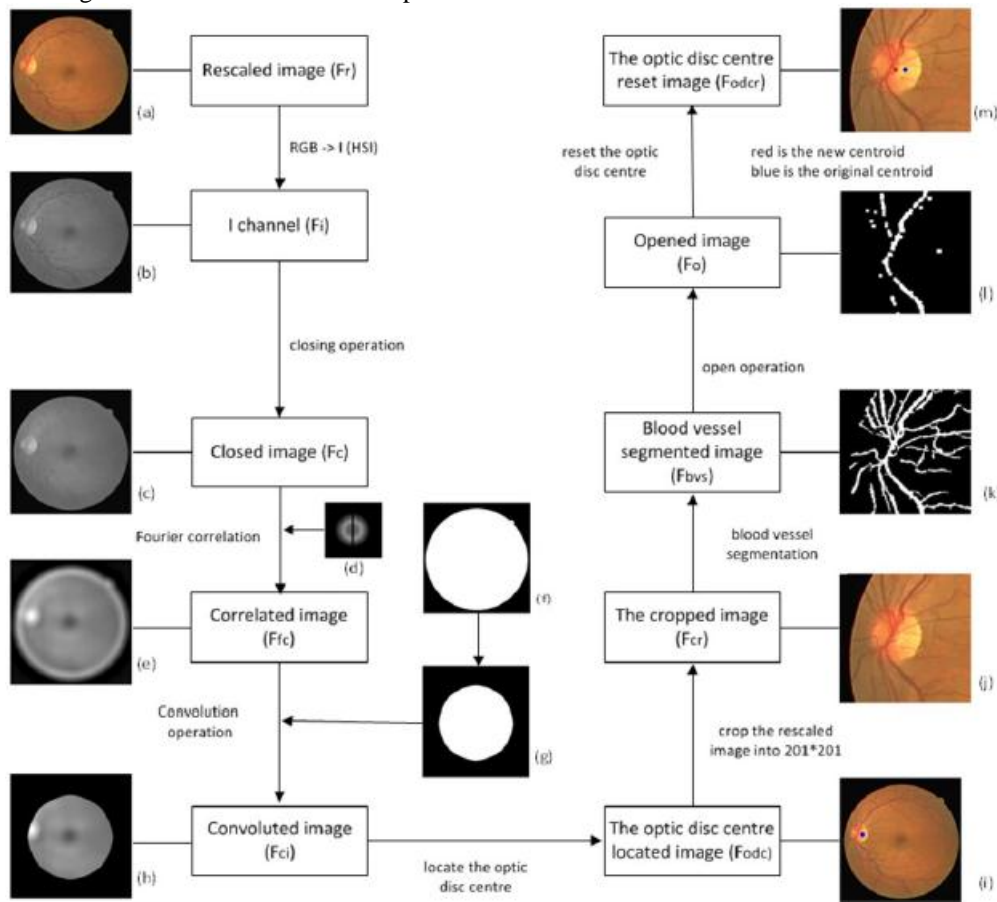

Figure 1.   The process to locate the optic disc centre. (a) Rescaled image (F_r). (b) The channel I image from F_r (F_i). (c) Closing operation of F_i (F_c). (d) The template (F_t) with the size of 201*201. (e) The Fourier correlated image from F_t and F_c (F_{fc}). (f) The mask of F_r (F_m). (g) The border eroded image from F_m (F_{be}). (h) The convoluted image from F_{fc} and F_{be} (F_{ci}). (i) The optic disc centre located image on F_r (F_{odc}). (j) The cropped image from F_r with the size of 201*201 (F_{cr}). (k) The blood vessel segmented image (F_{bvs}). (l) Open operation of F_{bvs} (F_o). (m) The optic disc centre reset image (F_{odcr}).

A.   Template Matching

Because the size of the optic disc varies from dataset to dataset, in order to make the size of it at the same scale, we rescale the size of the original retinal images into 570*760*3 (Fig. 1 (a)). The channel I (F_i), which contains the intensity information of F_r in the HSI colour space, is extracted to detect the optic disc centroid. Then, the morphological closing operation is applied to F_i to remove the blood vessels, and the closed image F_c is shown in Fig. 1 (c). A 201*201 size binary image is used as a template F_t (Fig. 1 (d)). This is followed by correlating F_t with F_c. In this work, the full Pearson-R

correlation is used to explain the variations of the mean intensity and contrast, the formulation is defined as:

$$C_{i,j} = \frac{\sum\limits_{x,y}(F_c(x,y)-\overline{F}_c(x,y))(F_t(x-i,y-j))-\overline{F}_t)}{\sum\limits_{x,y}(F_c(x,y)-\overline{F}_c(x,y))^2\sum\limits_{x,y}((F_t(x-i,y-j))-\overline{F}_t)^2} \quad (1)$$

where $\overline{F}_t$ and $\overline{F}_c$ are the mean value of F_t and the area covered by F_t, respectively. The correlated image (F_{fc}) is shown in Fig. 1 (e). The peak of F_{fc} is the approximate centre of the optic disc. However, it is obvious that the near-circular rim is with high intensity. In order to

214

eliminate the effect of the rim, an eroded image (see Fig. 1 (g)) is used to convolute with F_{fc} to remove the near circular rim area. The eroded image is obtained from the mask (Fig. 1 (f)) by using morphological erode operation. The Fig. 1 (h) shows the convoluted image (F_{ci}).

B. Locating the Optic Disc Centre

After the template matching method, the approximate centre of the optic disc is located by detecting the peak of F_{ci}. The optic disc centre located image (F_{odc}) is shown in Fig. 1 (i). This is followed by cropping F_r into 201*201*3 by using the peak as the centroid. Fig. 1 (j) shows the cropped image (F_{cr}). Due to the centre of the optic disc is usually located around the blood vessel and the Level Set Method is sensitive to the initialisation, the blood vessel information is extracted to reset the centroid. First, the closing operation is applied to the grey level image of F_r to remove the blood vessel. This is followed by calculating the difference between the closed image and the grey level image. Because of the low contrast of the difference image, the contrast adjustment function is used to enhance it. Then, a global threshold of the adjusted image is calculated, and the threshold method is applied to extract the blood vessel. The blood vessel segmented

image (F_{bvs}) is shown in Fig. 1 (k). After that, the morphological open operation is applied on F_{bvs} to prune small brunch and keep the main arcade, and Fig. 1 (l) shows the opened image (F_o). We let (c_x, c_y) as the approximate centre of the optic disc. According to the experiments, c_y is already located at the centroid of the optic disc. Therefore, we keep the y value of the approximate centre unchanged ($c_{y'}$) and find a new c_x value according to $F_o(c_{x'})$. The optic disc reset image (F_{odcr}) is shown in Fig. 1 (m), and the red point of the image is the reset centroid and the blue one is the original centre.

III. OPTIC DISC SEGMENTATION

We perform the segmentation using the grey level image F_{odcr}, which contains all the information necessary. However, the high contrast of the blood vessel inside the optic disc misguides the segmentation energy functional and breaks the continuity of the optic disc boundary. Therefore, we apply the morphological closing operation to remove the blood vessels, and the vessel removed image (F_{vr}) is obtained. Fig. 2 shows sample images before and after the closing operation.
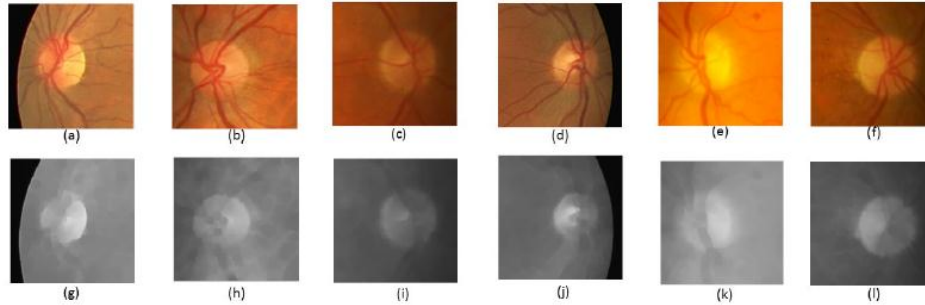

Figure 2. Morphological close operation on the cropped retinal images. The first row is the input images; the second row is the closed images.

Our aim is to segment the optic disc from (F_{vr}). Let Ω be the image domain and ϕ be a signed distance function (SDF). To obtain a better segmentation, we develop the energy functional as:

$$E(\phi) = E_S(\phi) + E_E(\phi) + E_R(\phi) \qquad (2)$$

Each terms of the energy functional model different aspects of the problem. The first term E_S is a shape prior term, which is used to compensate intensity inhomogeneity inside the optic disc due to the shadow after the blood vessel removal. The second term E_E incorporates the edge information derived from the vessel removed image, because the optic disc has significant edge information. The last term E_R is a distance regularization term, which keeps the optic disc boundary smooth.

A. Shape-prior Term

The shape-prior term was first introduced by Azadeh et al. [20]. Because the intensity inside the optic disc is inhomogeneity due to the residuals of vessel removal, the shape-prior term is incorporated to compensate intensity inhomogeneity inside the optic disc. Usually, the shape of the optic disc is circular. Therefore, a circular prior term

is applied to assist the algorithm when the edge term is insufficient to segment the optic disc boundary. The square distance from a point (x, y) to the shape constraining boundary is defined as:

$$D(x, y) = [(x - c_{x'})^2 + (y - c_{y'})^2 - r^2] \qquad (3)$$

where ($c_{x'}$, $c_{y'}$) is the optic disc centre and r is the approximate radius of the optic disc.

The circular prior term is used to encourage the boundary of the SDF ϕ to lie on the circular. Therefore, the shape term can be formulated as:

$$E_S(\phi) = \lambda_S \int_\Omega D(x, y)\delta_\epsilon(\phi(x, y)) \,|\, \nabla\phi(x, y)\,|dxdy \qquad (4)$$

where $\lambda_S \in \mathcal{R}$ is a constant coefficient, and δ_ϵ is the Dirac delta function. This term calculates the line integral of D along the zero level boundary of ϕ. It keeps the boundary of ϕ circular. The Dirac delta function δ is:

$$\delta_\epsilon(x) = \begin{cases} \dfrac{1}{2\epsilon}[1 + \cos(\dfrac{\pi x}{\epsilon})], & |x| \leq \epsilon \\ 0, & |x| > \epsilon. \end{cases} \qquad (5)$$

where ϵ is a constant parameter.

B. Edge-Based Term

In order to locate the boundary of the optic disc accurately, we incorporate the edge-based information into the energy formulation. The edge based term adapts the Chunming's model [21] and the energy functional is:

$$E_E(\phi) = \lambda L_g(\phi) + \alpha A_g(\phi) \qquad (6)$$

where $\lambda > 0$ and $\alpha \in \mathcal{R}$ are constant coefficients. The first term $L_g(\phi)$ calculates the line integral of the function g along the zero level boundary of ϕ. When the zero level set ϕ is on the optic disc boundaries, the edge-based term is minimised, while the function $A_g(\phi)$ computes the weighted area of the region $\phi(x,y) < 0$. This process is also used to speed up the motion of the zero level contours in the evolution process. More details can be found in [22]-[23]. The energy functional $L_g(\phi)$ and $A_g(\phi)$ are defined as:

$$L_g(\phi) \approx \int_\Omega g \delta_\epsilon(\phi(x,y)) \, | \nabla \phi(x,y) | \, dxdy \quad (7)$$

$$A_g(\phi) \approx \int_\Omega g H_\epsilon(-\phi(x,y)) dxdy \qquad (8)$$

where g and H_ϵ are the edge indicator function and the Heaviside function respectively. The edge indicator function is formulated by:

$$g \approx \frac{1}{1 + | \nabla G_\delta * I_m(x,y) |} \qquad (9)$$

where G_δ is the Gaussian kernel with a standard deviation δ. The indicator is used to smooth the image and reduce the noise through the convolution. The Heaviside function H is expressed as:

$$H_\epsilon(x) = \begin{cases} \frac{1}{2}[1 + \frac{x}{\epsilon} + \frac{1}{\pi}\sin(\frac{\pi x}{\epsilon})], & |x| \le \epsilon \\ 1, & x > \epsilon \\ 0, & x < \epsilon. \end{cases} \qquad (10)$$

C. Distance-Regularization Term

Since the boundary of the optic disc is located, we need to maintain the accuracy during the extraction by smoothing the boundary. Thus a distance regularization term is added to the energy functional, which is derived as:

$$E_R(\phi) = \lambda'_R E'_R(\phi) + \lambda''_R E''_R(\phi) \qquad (11)$$

where λ'_R and λ''_R are positive valued parameters. The first term $E'_R(\phi)$ computes the contour length of the zero level set ϕ to smooth the boundary of the optic disc.

However the penalty term from Chunming [24] is added to keep the zero level set ϕ close to the optic disc boundary. The equations of $E'_R(\phi)$ and $E''_R(\phi)$ are defined by:

$$E'_R(\phi) = \int_\Omega \delta_\epsilon(\phi(x,y)) \, | \nabla \phi(x,y) | \, dxdy \qquad (12)$$

$$E''_R(\phi) = \int_\Omega \frac{1}{2}(| \nabla \phi(x,y) | -1)^2 dxdy \qquad (13)$$

D. Energy Minimisation

The energy terms defined as (4), (6) and (11) is substituted into (2), and our energy model of $E(\phi)$ can be rewritten as:

$$\begin{aligned} E_\phi = &\lambda_S \int_\Omega D(x,y)\delta_\epsilon(\phi(x,y)) \, | \nabla \phi(x,y) | dxdy + \\ &\lambda \int_\Omega g\delta_\epsilon(\phi(x,y)) \, | \nabla \phi(x,y) | \, dxdy + \\ &\alpha \int_\Omega g H_\epsilon(-\phi(x,y)) dxdy + \\ &\lambda'_R \int_\Omega \delta_\epsilon(\phi(x,y)) \, | \nabla \phi(x,y) | \, dxdy + \\ &\lambda''_R \int_\Omega \frac{1}{2}(| \nabla \phi(x,y) | -1)^2 dxdy \end{aligned} \qquad (14)$$

In calculus of variations [25], minimizing the energy functional of $E(\phi)$ with respect to ϕ by using gradient decent method is as follows:

$$\frac{\partial \phi}{\partial t} = -\frac{\partial E(\phi)}{\partial \phi} \qquad (15)$$

where $\frac{\partial E(\phi)}{\partial \phi}$ is the *Gâteaux* derivative [25] of the energy function $E(\phi)$. The equation of (15) is derived by using Euler-Lagrange equations [26], which give us the gradient flow as follows

$$\begin{aligned} \frac{\partial \phi}{\partial t} = &\lambda_S(\nabla D | \nabla \phi | + D div(\frac{\nabla \phi}{|\nabla \phi|}))\delta_\epsilon(\phi) + \\ &\{\lambda(\nabla g | \nabla \phi | + g div(\frac{\nabla \phi}{|\nabla \phi|}) + \alpha g\}\delta_\epsilon(\phi) + \\ &\lambda'_R div(\frac{\nabla \phi}{|\nabla \phi|}) + \lambda''_R(4\triangle\phi - div(\frac{\nabla \phi}{|\nabla \phi|})) \end{aligned} \qquad (16)$$

where $div(\cdot)$ is the divergence operator, which is used to calculate the curvature of the evolving curve by using the spatial derivatives ϕ up to the second order.

IV. EXPERIMENTAL RESULTS

A. Dataset

The proposed method was evaluated on three public datasets, the DRIVE [27], the DIARETDB0 [28] and the DIARETDB1 [29], with a total of 259 images.

The DRIVE dataset includes 40 fundus images with 768*564 pixels and 8 bits per RGB channel, which were

captured by a Cannon CR5 non-mydriatic 3CCD camera at $45°$ field of view (FOV) and initially saved as JEPG-format. This database include two sets: a test and train set with 20 images each. Both sets have blood vessel hand-segmented images, and a second independent hand-label is also available for the test set.

The DIARETDB0 dataset consists of 130 colour images where 20 of them are normal and 110 of them contain signs of the diabetic retinopathy. These images were captured by few $50°$ FOV digital fundus cameras with unknown camera settings (flashing intensity, shutter speed, aperture, gain), and have a size of 1500*1152 pixels.

The DIARETDB1 dataset contains 89 retinal images, of which 84 have at least one indication of the diabetic retinopathy. The images were captured with a digital fundus camera at $50°$ FOV with varying imaging settings (flashing intensity, shutter speed, aperture, and gain). The size of the image is 1500*1152 pixels, 8 bits per RGB channel. In addition, the dataset provides ground truth on hard exudates, haemorrhages, red small dots and soft exudates by four experts, respectively.

All of the three datasets do not provide the ground truth for the optic disc. In order to evaluate the performance of the proposed segmentation method, we created the hand labelled sets for the three datasets according to the expert's guidance.

B. Performance Measures

Seven performance measurements are selected to evaluate different retinal extraction algorithms. Four of them are sensitivity (R_{sen}), specificity (R_{spe}), predictive value (P_v) and overlapping ratio (O_r), respectively. These metrics are defined as:

$$R_{sen} = \frac{N_{TP}}{N_{TP} + N_{FN}} \qquad R_{spe} = \frac{N_{TN}}{N_{TN} + N_{FP}}$$

$$P_v = \frac{N_{TP}}{N_{TP} + N_{FP}} \qquad O_r = \frac{area(A \cap B)}{area(A \cup B)} \qquad (17)$$

where N_{TP}, N_{FN}, N_{FP}, N_{TN} are the number of true positive,

false negative, false positive and true negative, respectively; A and B represent the optic disc region segmented by the human expert and our proposed method, respectively. The following expressions, TP is defined as all the vessel pixels that are labelled correctly, FP is all the non-vessel pixels that are wrongly labelled as vessel pixels, TN refers to as the non-vessel pixels which are correctly labelled and finally FN defines the vessel pixels that are wrongly labelled as non-vessel pixels. The sensitivity and specificity measures are calculated to show the percentage of true positive and true negative, respectively. Besides, the predictive value [30] is defined to illustrate the accuracy of the proposed method further. Finally, overlapping ratio of the optic disc region between the ground truth and the output of the proposed result is computed.

This is followed by computing the Euclidean distance between the optic disc centroid obtained by the proposed method and the centre of the ground truth region. The calculation of the Euclidean distance is:

$$ED(A, B) = \sqrt{(x_1 - x_2)^2 + (y_1 - y_2)^2} \qquad (18)$$

where (x_1, y_1) and (x_2, y_2) are the centroids of the A and B, respectively.

In addition, the mean absolute distance (MAD) between the optic disc boundary extracted by the proposed method and the ground truth is calculated as a measurement of detection accuracy [31]. The formulation of the MAD is defined as:

$$MAD(A_c, B_c) = \frac{1}{2} \{ \frac{1}{n} \sum_{i=1}^{n} d(a_i, B_c) + \frac{1}{m} \sum_{i=1}^{m} d(b_i, A_c) \} \qquad (19)$$

where A_c and B_c are sets of points from the optic disc contour of our segmentation method and ground truth, i.e. $A_c = \{a_1, a_2, \ldots, a_n\}$ and $B_c = \{b_1, b_2, \ldots, b_n\}$. Furthermore, $d(a_i, B_c)$ is the minimum distance from a_i to the set of points B_c. Finally, the last permanence measure is the computation time, which indicates the efficiency of the method.

TABLE I.   THE OPTIC DISC DETECTION PERFORMANCE ON THE DRIVE, DIARETDB0 AND DIARETDB1 DATASETS

Methods	Detection Performance (DRVIE dataset) (%)	Detection Performance (DIARETDB1dataset) (%)	Detection Performance (DIARETDB0dataset) (%)
Walter [30]	77.5	92.13	-
Sopharak [32]	95	59.55	-
Seo [33]	95	80.89	-
Kande [34]	95	86.51	-
Stapor [35]	87.5	78.65	-
Lupascu [36]	95	88.76	-
Welfer [37]	100	97.70	-
Our Method	100	97.75	97.70

C. Results

Table I shows the performance of the optic disc location on the DRIVE, DIARETDB0 and DIARETDB1 datasets. The performance of our method is compared with the alternative methods: Walter et al. [30], Sopharak *et al.* [32], Seo *et al.* [33], Kande *et al.* [34], Stapor *et al.*

[35], Lupascu *et al.* [36] and Welfer *et al.* [37] taken from [37]. The comparison indicates that the proposed method achieves the best performance in detecting the optic disc than alternative methods. This method can 100% detect the location of the optic disc on DRIVE dataset, 97.75% on DIARETDB1 dataset (2 out of 89 images), and 97.7% on DIARETDB0 dataset (3 out of 130 images). Welfer *et*

al. [37] obtains almost the same result as the template matching method on the DRIVE and DIARETDB1 datasets. The performances of the rest methods are all inferior to this method.

Table II compares the performance of the optic disc segmentation with the state of art methods: Walter *et al.* [30], Sopharak *et al.* [32], Seo *et al.* [33], Kande *et al.* [34], Stapor *et al.* [35], Lupascu *et al.* [36] and Welfer *et al.* [37] taken from [37]. All of the other methods are tested on two datasets: DRIVE and DIARETDB1 datasets only. We also use DIARETDB0 dataset to evaluate the performance of our method. Our method achieves

89.06% mean overlapping ratio, 94.65% mean sensitivity, 98.89% mean specificity, 93.95% average predictive value, 2.76 mean Euclidean distance and 2.48 mean absolute distance on the dataset.

The performance of optic disc segmentation on DRIVE dataset, our method with averages sensitivity 92.58%, predictive value 94.23%, overlapping ratio 88.16%, Euclidean distance 3.11 and mean absolute distance 2.52 outperforms all the alternative methods. However, the value of the average specificity achieves by our method is marginally inferior to other methods except Kande *et al.* [34] and Stapor *et al* [35].

TABLE II. THE OPTIC DISC SEGMENTATION PERFORMANCE ON DRIVE, DIARETDB0 AND DIARETDB1 DATASETS.

| Methods	Average Sensitivity (%)	Average Specificity (%)	Average Predictive value (%)	Average Overlap (%)	Average Euclidean distance	Average MAD	Average time per image (s)
DRIVE dataset							
Walter [30]	49.88	99.81	86.53	29.32	16.51	14.96	219.60
Sopharak[32]	21.04	99.93	93.34	16.88	20.85	23.15	14.92
Seo[33]	50.29	99.83	84.3	31.09	19.68	14.00	7.23
Kande[34]	69.99	98.88	52.18	29.66	29.66	12.49	111.74
Stapor[35]	73.68	99.20	61.98	33.42	11.12	7.5	43.00
Lupascu[36]	77.68	99.68	88.14	40.01	9.51	9.71	-
Welfer[37]	83.54	99.81	89.38	42.54	7.48	5.65	22.66
Our method	92.58	99.26	95.19	88.17	2.46	2.51	17.55
DIARETDB1 dataset							
Walter [30]	65.69	99.93	93.95	36.97	13.10	16.03	308.56
Sopharak[32]	46.03	99.94	95.93	29.41	6.99	16.86	74.55
Seo[33]	61.03	99.87	88.78	35.32	13.62	9.84	15.63
Kande[34]	88.08	98.78	54.48	33.41	21.77	8.50	120.55
Stapor[35]	84.98	99.64	80.34	34.08	6.74	6.03	59.72
Lupascu[36]	68.48	99.69	81.17	30.95	16.04	13.81	-
Welfer[37]	92.51	99.76	87.60	44.58	4.95	3.91	24.10
Our method	93.24	98.94	94.23	88.16	3.11	2.74	18.25
DIARETDB0 dataset							
Our method	94.65	98.89	93.95	89.06	2.76	2.48	18.3
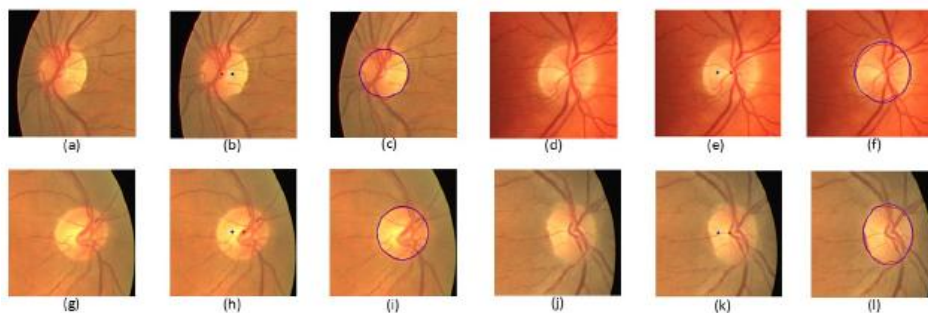
Figure 3.   The DRIVE dataset: (a, d, g, j) The cropped retinal images. (b, e, h, k) The optic disc centre reset images. (c, f, i, l) Our segmentation results (Red is our segmentation result, blue is the ground truth).
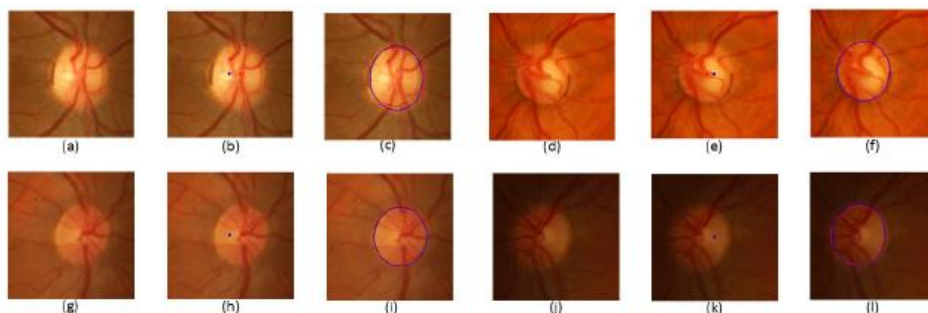

Figure 4.   The DIARETDB1 dataset: (a, d, g, j) The cropped retinal images. (b, e, h, k) The optic disc centre reset images. (c, f, i, l) Our segmentation results (Red is our segmentation result, blue is the ground truth).

218

Similarly to the DRIVE dataset, our method achieves the best overall performance on DIARETDB1 dataset. As we can see from the Table II, the proposed method outperforms all the other methods on averages sensitivity, predictive value, overlapping ratio, Euclidean distance and mean absolute distance respectively. Nevertheless our method achieves lower average specificity compared to the alternative methods.
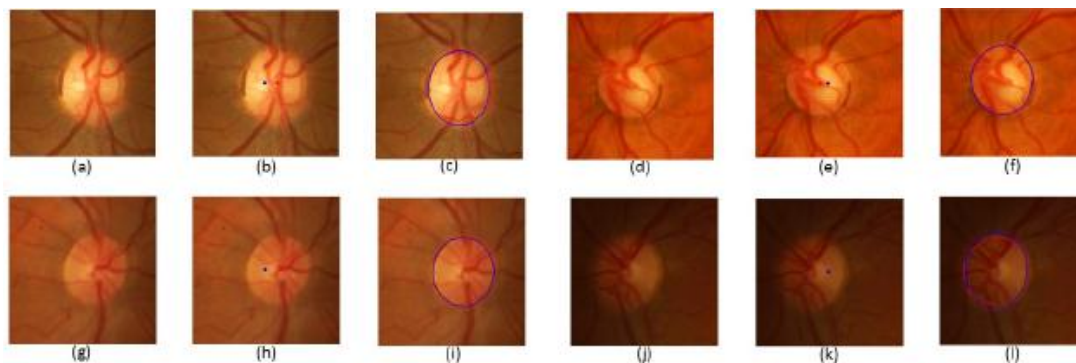
Fig. 3-Fig. 5 illustrate the output images of our proposed method and ground truth images for the DRIVE, DIARETDB1 and DIARETDB0 datasets, respectively.

Figure 5.   The DIARETDB0 dataset: (a, d, g, j) The cropped retinal images. (b, e, h, k) The optic disc centre reset images. (c, f, i, l) Our segmentation results (Red is our segmentation result, blue is the ground truth).

The proposed approach is implemented on MATLAB R2011b and the average computation time of our algorithm is 17.55 seconds for an image in the DRIVE dataset, 18.25 seconds for an image of DIARETDB1, and 18.3 seconds for an image of DIARETDB0 on Intel(R) Core(TM) i5-2500 CPU, clock of 3.3GHz, and 8G RAM memory.

V.   CONCLUSION

We have presented a novel method to detect and extract the optic disc from retinal images. First, the template matching method is used to approximately locate the position of the optic disc. Then, the morphological based method is applied to extract the blood vessels, and this information is used to reset the centroid of the optic disc. After that, the Level Set Method incorporated with shape-prior term, distance-regularization term and edge-based term is used to segment the optic disc.

The effectiveness of our method is evaluated against the-state-of-the-art methods on two publicly datasets: the DRIVE and DIARETDB1 datasets. Furthermore, the DIARETDB0 dataset is also used to evaluate the proposed method. The overall experimentation results show that the proposed method outperformed all the alternative methods we have compared with. Our method has advantages over the shape-based template matching method as it addresses the obstruction of the vessels inside the optic disc area and the intensity inhomogeneity, which generally affects the segmentation of the optic disc. Unlike the gradient based active contour methods, the model free snake methods and general region based active contour methods; our method can perform the segmentation of normal and irregular optic disc shape without affecting the optic disc shape constraints.

ACKNOWLEDGMENT

REFERENCES

[1]   R. JMJ, "Leading causes of blindness worldwide," *Bull. Soc. Belge Ophtalmol,* vol. 283, pp. 19-25, 2002.

[2]   R. Abdel-Ghafar and T. Morris, "Progress towards automated detection and characterization of the optic disc in glaucoma and diabetic retinopathy," *Informatics for Health and Social Care,* vol. 32, no. 1, pp. 19-25, 2007.

[3]   M. Lalonde, M. Beaulieu, and L. Gagnon, "Fast and robust optic disc detection using pyramidal decomposition and hausdorff-based template matching," *IEEE Transactions on Medical Imaging,* vol. 20, no. 11, pp. 1193-1200, 2001.

[4]   R. Chrastek, M. Wolf, K. Donath, G. Michelson, and H. Niemann, "Optic disc segmentation in retinal images," in *Bildverarbeitung Fur die Medizin*, Springer, 2002, pp. 263-266.

[5]   S. Sekhar, W. Al-Nuaimy, and A. K. Nandi, "Automated localisation of retinal optic disk using hough transform," in *Proc. 5th IEEE International Symposium on Biomedical Imaging: From Nano to Macro*, 2008.

[6]   X. Zhu and R. M. Rangayyan, "Detection of the optic disc in images of the retina using the hough transform," in *Proc. Engineering in Medicine and Biology Society, 30th Annual International Conference of the IEEE*, 2008.

[7]   P. Pallawala, W. Hsu, M. L. Lee, and K.-G. A. Eong, "Automated optic disc localization and contour detection using ellipse fitting and wavelet transform," in *Computer Vision-ECCV 2004*, Springer, 2004, pp. 139-151.

[8]   J. Lowell, A. Hunter, D. Steel, A. Basu, R. Ryder, E. Fletcher, and L. Kennedy, "Optic nerve head segmentation," *IEEE Trans. Med. Imaging,* vol. 23, no. 2, pp. 256-264, 2004.

[9]   A. Osareh, M. Mirmehdi, B. Thomas, and R. Markham, "Colour morphology and snakes for optic disc localisation," in *Proc. 6th Medical Image Understanding and Analysis Conference*, 2002.

[10] J. Novo, M. G. Penedo, and J. Santos, "Localisation of the optic disc by means of GA-optimised topological active nets," *Image and Vision Computing,* vol. 27, no. 10, pp. 1572-1584, 2009.

[11] D. Wong, J. Liu, J. Lim, X. Jia, F. Yin, H. Li, and T. Wong, "Level-set based automatic cup-to-disc ratio determination using retinal fundus images in ARGALI," in *Engineering in Medicine and Biology Society, 30th Annual International Conference of the IEEE*, 2008.

[12] J. Xu, O. Chutatape, E. Sung, C. Zheng, and P. Chew Tec Kuan, "Optic disk feature extraction via modified deformable model

technique for glaucoma analysis," *Pattern Recognition,* vol. 40, no. 7, pp. 2063-2076, 2007.

[13] H. Li and O. Chutatape, "Boundary detection of optic disk by a modified ASM method," *Pattern Recognition,* vol. 36, no. 9, pp. 2093-2104, 2003.

[14] H. Li and O. Chutatape, "Automated feature extraction in color retinal images by a model based approach," *IEEE Transactions on Biomedical Engineering,* vol. 51, no. 2, pp. 246-254, 2004.

[15] G. D. Joshi, J. Sivaswamy, and S. Krishnadas, "Optic disk and cup segmentation from monocular color retinal images for glaucoma assessment," *IEEE Transactions on Medical Imaging,* vol. 30, no. 6, pp. 1192-1205, 2011.

[16] D. Mumford and J. Shah, "Optimal approximations by piecewise smooth functions and associated variational problems," *Communications on Pure and Applied Mathematics,* vol. 42, no. 5, pp. 577-685, 1989.

[17] T. F. Chan and L. A. Vese, "Active contours without edges," *IEEE Transactions on Image Processing,* vol. 10, no. 2, pp. 266-277, 2001.

[18] G. D. Joshi, J. Sivaswamy, K. Karan, and S. Krishnadas, "Optic disk and cup boundary detection using regional information," in *Proc. International Symposium on Biomedical Imaging: From Nano to Macro,* 2010.

[19] Y. Tang, X. Li, A. von Freyberg, and G. Goch, "Automatic segmentation of the papilla in a fundus image based on the C-V model and a shape restraint," in *Proc. 18th International Conference on Pattern Recognition*, 2006.

[20] A. Mishra, A. Wong, K. Bizheva, and D. A. Clausi, "Intra-retinal layer segmentation in optical coherence tomography images," *Opt. Express,* vol. 17, no. 26, pp. 23719-23728, 2009.

[21] C. Li, C. Xu, C. Gui, and M. D. Fox, "Distance regularized level set evolution and its application to image segmentation," *IEEE Trans. on Image Process.,* vol. 19, no. 12, pp. 3243-3254, 2010.

[22] V. Caselles, R. Kimmel, and G. Sapiro, "Geodesic active contours," *Int. J Comput. Vis.,* vol. 22, no. 1, pp. 61-79, 1997.

[23] H.-K. Zhao, T. Chan, B. Merriman, and S. Osher, "A variational level set approach to multiphase motion," *J. Comput. Phys.,* vol. 127, no. 1, pp. 179-195, 1996.

[24] C. Li, C. Xu, C. Gui, and M. D. Fox, "Level set evolution without re-initialization: a new variational formulation," in *Comput. Vis. and Pattern Recognition, IEEE Comput. Society Conf.*, 2005.

[25] G. Aubert and P. Kornprobst, Mathematical problems in image processing: Partial differential equations and the calculus of variations, vol. 147, Springer, 2006.

[26] B. Smith, A. Saad, G. Hamarneh, and T. Mller, "Recovery of dynamic PET regions via simultaenous segmentation and deconvolution," in *MICCAI Workshop on Analysis of Functional Medical Image Data (MICCAI Functional)*, 2008.

[27] J. Staal, M. D. Abrmoff, M. Niemeijer, M. A. Viergever, and B. van ginneken, "Ridge-based vessel segmentation in color images of the retina," *IEEE Trans. Med. Imaging,* vol. 23, no. 4, pp. 501-509, 2004.

[28] T. Kauppi, V. Kalesnykiene, J.-K. Kamarainen, L. Lensu, I. Sorri, *et al.*, "DIARETDB0: Evaluation database and methodology for diabetic retinopathy algorithms," *Machine Vis. Pattern Recognition Research Group, Lappeenranta Uni. Technology, Finland,* 2006.

[29] T. Kauppi, V. Kalesnykiene, J.-K. Kamarainen, L. Lensu, I. Sorri, A. Raninen, *et al.*, "The DIARETDB1 diabetic retinopathy database and evaluation protocol," in *BMVC*, 2007.

[30] T. Walter, J.-C. Klein, P. Massin, and A. Erginay, "A contribution of image processing to the diagnosis of diabetic retinopathy-detection of exudates in color fundus images of the human retina," *IEEE Trans. Med. Imaging,,* vol. 21, no. 10, pp. 1236-1243, 2002.

[31] V. Chalana, D. T. Linker, D. R. Haynor, and Y. Kim, "A multiple active contour model for cardiac boundary detection on echocardiographic sequences," *IEEE Trans. Med. Imaging,* vol. 15, no. 3, pp. 290-298, 1996.

[32] A. Sopharak, B. Uyyanonvara, S. Barman, and T. H. Williamson, "Automatic detection of diabetic retinopathy exudates from non-dilated retinal images using mathematical morphology methods," *Computerized Medical Imaging and Graphics,* vol. 32, no. 8, pp. 720-727, 2008.

[33] J. Seo, K. Kim, J. Kim, K. Park, and H. Chung, "Measurement of ocular torsion using digital fundus image," in *Proc. Engineering in Medicine and Biology Society, 26th Annual International Conference of the IEEE*, 2004.

[34] G. B. Kande, P. V. Subbaiah, and T. Satya Savithri, "Segmentation of exudates and optic disk in retinal images," in *Proc. Sixth Indian Conference on Computer Vision, Graphics & Image Processing*, 2008.

[35] K. Stapor, A. Witonski, R. Chrastek, and G. Michelson, "Segmentation of fundus eye images using methods of mathematical morphology for glaucoma diagnosis," in *Proc. Computational Science-ICCS*, Springer, 2004, pp. 41-48.

[36] C. A. Lupascu, D. Tegolo, and L. Di Rosa, "Automated detection of optic disc location in retinal images," in *Proc. 21st IEEE International Symposium on Computer-Based Medical Systems*, 2008.

[37] D. Welfer, J. Scharcanski, and D. R. Marinho, "A morphologic two-stage approach for automated optic disk detection in color eye fundus images," *Pattern Recognition Letters*, 2012.

Chuang Wang received the B.Eng. degree in electronics information engineering from University of Science and Technology Liao Ning, Liao Ning, China, in 2009, and the M.Eng. degree in Electrical Engineering from Pusan National University, Busan, South Korea, in 2011. He is currently working toward the Ph.D. degree in the Department of Computer Science, Brunel University, London, U.K.

Since 2012, he has been a Teaching Assistant in the Department of Computer Science, Brunel University, London, U.K. His research interests include H.264 encoder and decoder, computer vision, medical image analysis, pattern recognition, and machine learning.

Djibril Kaba received the M.Eng. and B.Eng. degrees in electronics engineering from Kings' College University, London, U.K., in 2010. He is currently working toward the Ph.D. degree in the Department of Computer Science, Brunel University, West London, U.K.

From 2010 to 2011, he worked as a Business Analyst for ITSeven, London, U.K. Since 2011, he has been a Teaching Assistant in the Department of Computer Science, Brunel University, London, U.K. His research interests include computer vision, image processing, pattern recognition, medical image analysis, and machine learning.
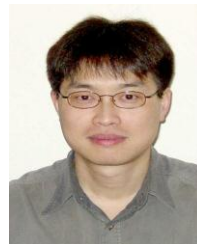
Yongmin Li received the M.Eng. and B.Eng. degrees in control engineering from Tsinghua University, Beijing, China, in 1990 and 1992, respectively, and the Ph.D. degree in computer vision from Queen Mary University of London, London, U.K., in 2001.

Between 2001 and 2003, he worked as a Research Scientist at the British Telecom Laboratories, Suffolk, U.K. He is currently a Senior Lecturer in the Department of Computer Science, Brunel University, West London, U.K. His current research interests include automatic control, nonlinear filtering, computer vision, image processing, video analysis, medical imaging, machine learning, and pattern recognition.